

Simple method for calculating the propagation of terahertz radiation in experimental geometries

D. Côté, J. E. Sipe, and H. M. van Driel

Department of Physics, University of Toronto, Toronto, Ontario M5S 1A7, Canada

Received August 28, 2002; revised manuscript received January 20, 2003

A formalism based on plane-wave decomposition is applied to the linear propagation of terahertz pulses in experimental geometries. The approach is general and is not restricted to any particular polarization (or current) source. Near- and far-field expressions easily amenable to numerical computation are obtained for the temporal profiles and spectra of terahertz pulses in layered structures, as often encountered in experiments. The effects of polarization and angle-dependent multiple reflection and transmission, as well as of material dispersion, are included. Examples of optical rectification in GaAs and ZnTe are presented to illustrate the simplicity of the method and are compared with experiments. The numerical evaluation of the expressions for the terahertz electric field in practical experimental geometries is straightforward. © 2003 Optical Society of America

OCIS codes: 050.1940, 320.7100, 320.7120, 350.5500, 350.5610.

1. INTRODUCTION

The temporal profile of an electromagnetic wave often carries important information about the source that generated the wave. A description of the effects of propagation on the temporal profile of such waves is often critical both in determining what information can be extracted from the measurements of the temporal profile and in extracting it. For experiments with simple boundary conditions,¹ the properties of the radiation can be studied analytically. In more-specialized applications, however, to extend the reach of analytical methods it is necessary to use approaches that allow some approximations to be made. In optics, for instance, one can use the paraxial wave equation to study the propagation of radiation in free space and thereby derive important analytical expressions for the beam properties.² However, recent advances in the production of few-cycle ultrashort optical pulses³ and terahertz (THz) pulses^{4–6} have permitted the creation of electromagnetic pulses that cannot be described by the paraxial wave equation. These pulses are often used in situations when the phases of different frequency components with respect to the envelope function are critical. Experimental techniques have been developed to time resolve the amplitude and phase of this radiation.^{4,7,8} It has been shown that the respective time signatures of this radiation in the near field and in the far field are vastly different.^{9–11} The full solution of Kirchhoff's diffraction integral has been used to model some experiments and has yielded excellent agreement with experimental data.¹² Yet the generalization of this formalism to more-complicated geometries, including interfaces, is not straightforward. And, whereas solving Maxwell equations with finite-difference techniques is always an option, doing so can be difficult, particularly in three dimensions.¹³

Our goal in this paper is to introduce a practical

method for calculating radiated fields from any prescribed source, in both the near and the far fields, such that an easy comparison of predicted results with experimental data can be achieved. This method permits the extraction of important details about the dynamics of the source that generated the radiation.¹⁴ In this study the propagation of broadband THz radiation in experimental situations is modeled; polarization-dependent effects at interfaces, multiple reflections, and dispersion of the index of refraction as well as near- and far-field pulse reshaping effects are taken into consideration. Sipe¹⁵ has shown that a plane-wave decomposition of the field permits a description of the propagation in both the near and the far fields in terms of simple, intuitive Green functions. The framework makes use of well-known results from linear optics (e.g., complete frequency-dependent Fresnel transmission and reflection coefficients) and lends itself nicely to an analysis of relatively complex geometries with multiple reflections and arbitrary polarizations, as are found in most practical studies.

The structure of this paper is as follows: In Section 2 we build on earlier research¹⁵ and introduce the formalism and notation. Next, in Section 3, we describe the propagation of radiation through vacuum, dielectric media, and lenses. We then use the results in Section 4 to obtain the Green functions for several geometries and calculate the radiation from an arbitrary polarization source. Finally, straightforward examples from realistic situations in both the near and the far fields are worked out, the results of which can be directly used in modeling most experimental situations.

2. FORMALISM

Plane waves and spherical waves are both eigenmodes of the Helmholtz equation. Therefore any propagating elec-

tromagnetic field can be expressed as a superposition of either plane or spherical waves. The key advantage in using plane waves rather than spherical waves is that the description of transmission and reflection at interfaces takes a simple form, in that the \hat{s} - and \hat{p} -polarized components of the field can usually be treated independently. Expressions for the propagation through any layered medium, by use of results from thin-film optics, can then easily be obtained. For these reasons we employ a plane-wave basis with polarization vectors \hat{s} and \hat{p} . Each plane wave is fully defined by four parameters: its frequency Ω , its wave vector $\boldsymbol{\nu}$, its polarization vector (\hat{s} or \hat{p}), and, finally, its complex amplitude. The wave vector $\boldsymbol{\nu}$ is further decomposed into two components, $\pm w$ (possibly complex) along the axial direction \hat{z} and \mathbf{K} (always real) in the xy plane transverse to \hat{z} . The vector $\mathbf{R} = R\hat{R} = x\hat{x} + y\hat{y}$ spans this transverse plane; the position vector in three dimensions is $\mathbf{r} = x\hat{x} + y\hat{y} + z\hat{z} = \mathbf{R} + z\hat{z}$. A plane-wave distribution is denoted by the Fourier spectral density $\mathbf{E}(\Omega, \mathbf{K})$. In an infinite medium with no sources, the field that results from the superposition of such plane waves that, together with the associated magnetic field, satisfies the Maxwell equations takes the form

$$\begin{aligned} \mathcal{E}(\mathbf{r}, t) = & \int_0^\infty \frac{d\Omega}{2\pi} \int \frac{d\mathbf{K}}{(2\pi)^2} \mathbf{E}(\Omega, \mathbf{K}; z) \exp(i\mathbf{K} \cdot \mathbf{R}) \\ & \times \exp(-i\Omega t) + \text{c.c.}, \end{aligned} \quad (1)$$

where

$$\mathbf{E}(\Omega, \mathbf{K}; z) = \mathbf{E}_+(\Omega, \mathbf{K}; z) + \mathbf{E}_-(\Omega, \mathbf{K}; z), \quad (2)$$

$$\mathbf{E}_\pm(\Omega, \mathbf{K}; z) = \mathbf{E}_\pm(\Omega, \mathbf{K}) \exp(\pm iwz), \quad (3)$$

$$\mathbf{E}_\pm(\Omega, \mathbf{K}) = \hat{s} E_\pm^s(\Omega, \mathbf{K}) + \hat{p}_\pm E_\pm^{p\pm}(\Omega, \mathbf{K}), \quad (4)$$

where a subscript \pm is now used to denote the $\pm\hat{z}$ direction in which the field is either propagating or suffering evanescent decay with wave-number component $\pm w$ along the axial direction. We refer generally to the $+$ ($-$) component as the upward- (downward-) propagating wave. For example, the distribution representing an upward-propagating plane wave of complex amplitude $\mathbf{E}_+^{\Omega, \mathbf{K}}$ at $z = z_0$ would be represented by

$$\mathbf{E}_+(\Omega, \mathbf{K}; z_0) = \mathbf{E}_+^{\Omega, \mathbf{K}} \delta(\Omega - \Omega_0) \delta(\mathbf{K} - \mathbf{K}_0), \quad (5)$$

where $\delta(x)$ denotes the Dirac delta distribution. The wave and polarization vectors are sketched in Fig. 1 for a situation in which they are real. More generally, in an isotropic medium they are given by

$$\boldsymbol{\nu}_\pm \equiv \mathbf{K} \pm w\hat{z}, \quad (6)$$

$$w \equiv (\tilde{\Omega}^2 n^2 - K^2)^{1/2}, \quad (7)$$

$$\hat{s} \equiv \hat{K} \times \hat{z}, \quad (8)$$

$$\hat{p}_\pm \equiv \nu^{-1}(K\hat{z} \mp w\hat{K}), \quad (9)$$

where $\boldsymbol{\nu}_\pm = \nu\hat{\nu}_\pm$ is the wave vector with wave number $\nu = \tilde{\Omega}n$; $\tilde{\Omega} \equiv \Omega/c$, where c is the speed of light; n is the (in general complex) index of refraction; $\mathbf{K} = K\hat{K}$ is the transverse component of the wave vector; and the square roots of complex numbers z are defined such that $\text{Im} \sqrt{z} \geq 0$ and that $\text{Re} \sqrt{z} \geq 0$ if $\text{Im} \sqrt{z} = 0$. Throughout, we

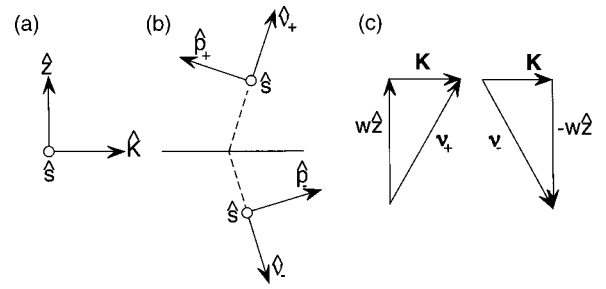


Fig. 1. Coordinate systems used in the calculations, sketched for \hat{s} , \hat{p}_\pm , and $\boldsymbol{\nu}_\pm$ real. (a) Axial direction \hat{z} , wave-vector component \mathbf{K} , and polarization \hat{s} . (b) Polarization vectors \hat{s} and \hat{p}_\pm for plane-wave directions $\hat{\nu}_\pm$. (c) Vector decomposition of plane-wave vector $\boldsymbol{\nu}_\pm$ into its transverse (\mathbf{K}) and axial ($\pm w\hat{z}$) components.

use subscripts, such as in w_i and $\hat{p}_{i\pm}$, to denote the indicated parameters in a medium of refractive index n_i . It should be noted that for an upward-propagating plane wave, given Ω and \mathbf{K} , one knows the direction $\hat{\nu}_\pm$ of the propagation vector through Eqs. (6) and (7) and that the direction depends on the index of refraction of the medium, n_i .

3. PROPAGATION AND TRANSFORMATIONS

In realistic experimental geometries, THz pulses propagate through air, dielectric media, and collimating optics. In as much as we are interested in the linear propagation of THz pulses we can describe the transformation of a single plane wave through such media and optics and reconstruct the transformation of a THz pulse from a superposition of plane waves. We now introduce the necessary transformations of plane waves through dielectric media and through lenses.

A. Free Space and Dielectrics

In vacuum, dielectric, or any layered media for which the interfaces are parallel to the xy plane, a plane wave always remains a plane wave or a sum of plane waves with the same wave vector component \mathbf{K} . The propagation of the fields is facilitated by the use of transfer matrices. A host of conventions are in common use.¹⁶ For positive frequency Ω , we find it convenient to define the matrices with respect to formal vectors $e_i(z)$ of the form

$$e_i(z) = \begin{bmatrix} E_+(\Omega, \mathbf{K}) \exp(iw_i z) \\ E_-(\Omega, \mathbf{K}) \exp(-iw_i z) \end{bmatrix}, \quad (10)$$

where we consider a medium with index of refraction n_i . Here $E_\pm(\Omega, \mathbf{K})$ identifies either $E_\pm^s(\Omega, \mathbf{K})$ or $E_\pm^{p\pm}(\Omega, \mathbf{K})$. Separate formal vectors $e_i(z)$ are used for \hat{s} - and \hat{p} -polarized light because the effects of interfaces on the propagation of those two polarizations can be treated independently. The transfer matrix $M_i(z)$ that transforms the formal vector of Eq. (10) on propagation in a uniform isotropic medium is

$$M_i(z) = \begin{bmatrix} \exp(iw_i z) & 0 \\ 0 & \exp(-iw_i z) \end{bmatrix}, \quad (11)$$

i.e., $e_i(z_1) = M_{ij}(z_1 - z_2)e_j(z_2)$ if z_1 and z_2 are in the same medium. The matrix M_{ij} for passage through an interface that separates media i and j takes the same form for either \hat{s} - or \hat{p} -polarized radiation; it is

$$M_{ij} = \frac{1}{t_{ij}} \begin{bmatrix} 1 & r_{ij} \\ r_{ij} & 1 \end{bmatrix}, \quad (12)$$

i.e., $e_i(z_o^+) = M_{ij}e_j(z_o^-)$ if medium i exists at $z > z_o$ and medium j at $z < z_o$, where the Fresnel coefficients for \hat{s} and \hat{p} polarizations are

$$r_{ij}^p = \frac{w_i n_j^2 - w_j n_i^2}{w_i n_j^2 + w_j n_i^2}, \quad r_{ij}^s = \frac{w_i - w_j}{w_i + w_j}, \quad (13)$$

$$t_{ij}^p = \frac{2n_i n_j w_i}{w_i n_j^2 + w_j n_i^2}, \quad t_{ij}^s = \frac{2w_i}{w_i + w_j}. \quad (14)$$

Now that basic propagation in dielectric media has been described, we shall examine the case in which a lens is in the path of the beam.

B. Thin Lens

If the refractive index of a lens is not too large and if the lens is not too small, one achieves a good approximation of the effect of the lens on a beam of light by modeling it as a phase mask locally affecting each ray that propagates

0 if $R > L$, with a corresponding distance in vacuum $d_{\text{vac}}(R) = R^2/2\tilde{R}$ if $R < L$ and D_L if $R > L$. Hence, within the usual approximations,¹⁷ at $z = d_o + D_L$ the input plane wave has acquired a phase as a function of radial distance R and is now described by

$$\begin{aligned} \mathcal{E}(\mathbf{R} + [d_o + D_L]\hat{z}, t) \\ = \mathbf{E}_+^{\Omega_o, \mathbf{K}_o} \exp[iw_{\text{vac}}d_{\text{vac}}(\mathbf{R}) \\ + iw_{\text{lens}}d_{\text{lens}}(\mathbf{R}) + i\mathbf{K}_o \cdot \mathbf{R} - i\Omega_o t] + \text{c.c.}, \end{aligned} \quad (15)$$

where w_{lens} (w_{vac}) is the z component of the wave vector inside (outside) the lens material. Reflections from any of the interfaces as well as polarization-dependent refraction effects are neglected. The output wave is clearly no longer a plane wave because of the R dependence imprinted on its phase. Thus, at $z = d_o + D_L$, an incident plane wave of transverse wave vector \mathbf{K}_o has become a distribution of plane waves $\mathbf{E}_+(\Omega, \mathbf{K}'; d_o + D_L)$:

$$\begin{aligned} \mathcal{E}(\mathbf{R} + [d_o + D_L]\hat{z}, t) \\ = \int_0^\infty \frac{d\Omega}{2\pi} \int \frac{d\mathbf{K}'}{(2\pi)^2} \mathbf{E}_+(\Omega, \mathbf{K}'; d_o + D_L) \\ \times \exp(i\mathbf{K}' \cdot \mathbf{R} - i\Omega t) + \text{c.c.}, \end{aligned} \quad (16)$$

with

$$\mathcal{E}(\mathbf{R} + [d_o + D_L]\hat{z}, t) = \begin{cases} \mathbf{E}_+^{\Omega_o, \mathbf{K}_o} \exp(-i\Delta w R^2/2\tilde{R} + iw_{\text{lens}}D_L + i\mathbf{K}_o \cdot \mathbf{R} - i\Omega_o t) + \text{c.c.} & R < L \\ \mathbf{E}_+^{\Omega_o, \mathbf{K}_o} \exp(iw_{\text{vac}}D_L + i\mathbf{K}_o \cdot \mathbf{R} - i\Omega_o t) + \text{c.c.} & R > L \end{cases}, \quad (17)$$

through it.¹⁷ Consider first a wave distribution incident from $z < d_o$ with Fourier spectrum $\mathbf{E}_+(\Omega, \mathbf{K}; d_o^-) = \mathbf{E}_+^{\Omega_o, \mathbf{K}_o} \delta(\Omega - \Omega_o) \delta(\mathbf{K} - \mathbf{K}_o)$ at $z = d_o^-$ on a parabolic lens of total thickness D_L , width $2L$, radius of curvature $\tilde{R} = R_o$, and index of refraction n , as shown in Fig. 2. Recall that this represents a plane wave with transverse wave vector \mathbf{K}_o , frequency Ω_o , and vector amplitude $\mathbf{E}_+^{\Omega_o, \mathbf{K}_o}$. The thickness of the lens as a function of radial distance is $d_{\text{lens}}(R) = D_L - R^2/2\tilde{R}$ if $R < L$ and

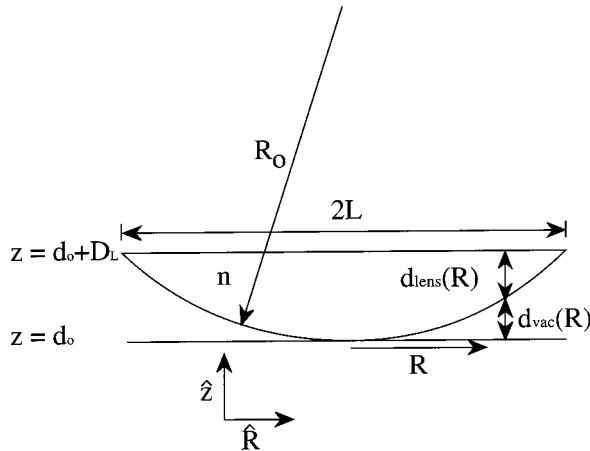


Fig. 2. Lens geometry used in the calculation. The upward-propagating beam is incident from $z < d_o$.

where $\Delta w = w_{\text{lens}} - w_{\text{vac}}$. One easily extracts the distribution $\mathbf{E}_+(\Omega, \mathbf{K}'; d_o + D_L)$ with an inverse Fourier transform of Eqs. (15) and (16):

$$\begin{aligned} \mathbf{E}_+(\Omega, \mathbf{K}'; d_o + D_L) \\ = \mathbf{E}_+^{\Omega_o, \mathbf{K}_o} \delta(\Omega - \Omega_o) \left\{ \exp(iw_{\text{lens}}D_L) \int_{R < L} d\mathbf{R} \right. \\ \times \exp[i(\mathbf{K}_o - \mathbf{K}') \cdot \mathbf{R} - i\Delta w R^2/2\tilde{R}] \\ \left. + \exp(iw_{\text{vac}}D_L) \int_{R > L} d\mathbf{R} \exp[i(\mathbf{K}_o - \mathbf{K}') \cdot \mathbf{R}] \right\}. \end{aligned} \quad (18)$$

As can be seen from Eq. (18), a single plane wave will exhibit diffraction rings after it has propagated through the lens because of the effect of the edge of the lens. Similarly, superpositions of plane waves that result in spatial profiles larger than the lens itself will not be properly focused or collimated and will therefore be attenuated. We can simplify the mathematical expressions and keep essentially the same attenuation effect as in Eq. (18) if, instead of a finite lens of half-width L , a Gaussian aperture (or soft aperture) of $1/e$ half-width $\sqrt{2}L$ (in amplitude) is assumed. The width of the soft aperture is defined such that the energy of a plane wave after the lens

is the same as what it would be were it a hard aperture. One can easily show that Eq. (15) with a complex radius of curvature

$$\frac{1}{\tilde{R}} = \frac{1}{R_o} - \frac{i}{\Delta w L^2} \quad (19)$$

represents a Gaussian aperture of half-width $\sqrt{2}L$, where R_o is the real radius of curvature of the lens. Using the shorthand notation

$$K_L^2 = \frac{2\Delta w}{R_o} - \frac{2i}{L^2}, \quad (20)$$

we can then approximate Eq. (18) by

$$\begin{aligned} \mathbf{E}_+(\Omega, \mathbf{K}'; d_o + D_L) &\approx \mathbf{E}_+^{\Omega_o, \mathbf{K}_o} \delta(\Omega - \Omega_o) \exp(i\Delta w D_L) \int d\mathbf{R} \\ &\times \exp[i(\mathbf{K}_o - \mathbf{K}') \cdot \mathbf{R}] \exp\left(-i \frac{R^2 K_L^2}{4}\right) \quad (21) \\ &= \frac{4\pi i}{K_L^2} \mathbf{E}_+^{\Omega_o, \mathbf{K}_o} \delta(\Omega - \Omega_o) \\ &\times \exp\left(i \frac{|\mathbf{K}_o - \mathbf{K}'|^2}{K_L^2} + i\Delta w D_L\right), \quad (22) \end{aligned}$$

where the integral has been performed by use of the identity¹⁸

$$\int_0^{2\pi} d\phi \exp(im\phi) \exp(ix \cos \phi) = 2\pi i^m J_m(x), \quad (23)$$

where $J_m(x)$ is the Bessel function of order m , as well as

$$\int_0^\infty R dR \exp(iaR^2) J_0(bR) = \frac{i}{2a} \exp\left(\frac{-ib^2}{4a}\right). \quad (24)$$

If a distribution of waves $\mathbf{E}_+(\Omega, \mathbf{K}; d_o^-)$ is incident upon the lens, the resultant distribution behind the lens is obtained by superposition:

$$\begin{aligned} \mathbf{E}_+(\Omega, \mathbf{K}'; d_o^+) &= \frac{4\pi i}{K_L^2} \int \frac{d\mathbf{K}}{(2\pi)^2} \mathbf{E}_+(\Omega, \mathbf{K}; d_o^-) \\ &\times \exp\left(i \frac{|\mathbf{K} - \mathbf{K}'|^2}{K_L^2}\right), \quad (25) \end{aligned}$$

where we have taken the thin lens limit where $D_L \rightarrow 0^+$. Equations (20) and (25) can be used to implement the lens transformation numerically. However, it is shown in Section 5 below that the transformation that corresponds to a common experimental geometry in which a Gaussian beam is collimated and refocused can be treated analytically.

4. SOURCES, GREEN FUNCTION, AND GEOMETRY

Although we have described the propagation of THz radiation in dielectric media and lenses, we have not discussed the generation of the radiation itself. From standard electromagnetic theory, it is known that

electromagnetic fields are radiated from oscillating currents. With any current density $\mathcal{J}(\mathbf{r}, t)$, we can associate a polarization potential (or density) according to $\mathcal{J}(\mathbf{r}, t) = \partial \mathcal{P}(\mathbf{r}, t) / \partial t$. Obtaining the radiated electric field for a given polarization density $\mathcal{P}(\mathbf{r}, t)$ is a boundary condition problem and depends on the geometry of the system under study. For instance, if source $\mathcal{P}(\mathbf{r}, t)$ is embedded in a dielectric medium with interfaces to other media, there will be multiple Fresnel reflections of the generated waves that will interfere inside and outside the dielectric material and affect the resultant radiation spectrum and profile. If the polarization source is described in terms of $\mathbf{P}(\Omega, \mathbf{K}; z)$ such that

$$\begin{aligned} \mathcal{P}(\mathbf{r}, t) &= \int_0^\infty \frac{d\Omega}{2\pi} \int \frac{d\mathbf{K}}{(2\pi)^2} \mathbf{P}(\Omega, \mathbf{K}; z) \exp(i\mathbf{K} \cdot \mathbf{R}) \\ &\times \exp(-i\Omega t) + \text{c.c.}, \quad (26) \end{aligned}$$

the radiated field is obtained in general from the following Green function integral:

$$\mathbf{E}(\Omega, \mathbf{K}; z) = \int dz' \tilde{G}(\Omega, \mathbf{K}; z - z') \cdot \mathbf{P}(\Omega, \mathbf{K}; z'). \quad (27)$$

In an infinite medium of index n_1 , the Green function in MKS units, is¹⁵

$$\begin{aligned} \tilde{G}(\Omega, \mathbf{K}; z) &= \frac{i\tilde{\Omega}^2}{2\epsilon_o w_1} (\hat{s}\hat{s} + \hat{p}_{1+}\hat{p}_{1+}) \theta(z) \exp(iw_1 z) \\ &+ \frac{i\tilde{\Omega}^2}{2\epsilon_o w_1} (\hat{s}\hat{s} + \hat{p}_{1-}\hat{p}_{1-}) \theta(-z) \\ &\times \exp(-iw_1 z) - \frac{1}{n_1^2 \epsilon_o} \hat{z}\hat{z} \delta(z), \quad (28) \end{aligned}$$

with Heaviside function $\theta(z) = 1, 0$ for $z > 0, < 0$ and where ϵ_o is the permittivity of free space. The right-hand side of Eq. (28) has terms that represent the upward- [$\exp(iw_1 z)$] and the downward- [$\exp(-iw_1 z)$] propagating (or evanescent) waves originating from a polarization density $\mathbf{P}(\Omega, \mathbf{K}; z')$ at z' for both \hat{s} and $\hat{p}_{1\pm}$ polarizations as well as a local term that will not be relevant for this study and that was discussed earlier.¹⁵ For an arbitrary geometry with a source embedded in a dielectric, one uses the results from Section 3 to obtain the Green function for any polarization source embedded in any layered dielectric structure.

A common geometry is shown in Fig. 3, where two semi-infinite dielectric materials, with indices of refraction n_1 and n_2 (which can be frequency dependent), are shown on either side of a third material, with index of refraction n_3 and thickness D . When the polarization

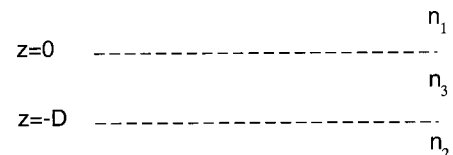


Fig. 3. Three-layer geometry with polarization source in the medium with index n_3 .

source is contained in medium 3, the expression for the upward-propagating radiation in medium 1 for $z > 0$ is given by¹⁵

$$\begin{aligned} \mathbf{E}_+(\Omega, \mathbf{K}; z) &= \frac{i\tilde{\Omega}^2}{2\epsilon_3 w_3} \sum_{\hat{q}} \mathcal{C}^q \exp(iw_1 z) \\ &\times \left[\hat{q}_{1+}\hat{q}_{3+} \cdot \int_{-\infty}^0 dz' \exp(-iw_2 z') \right. \\ &\times \mathbf{P}(\Omega, \mathbf{K}; z') + r_{32}^q \exp(2iw_3 D) \hat{q}_{1+}\hat{q}_{3-} \\ &\left. \cdot \int_{-D}^0 dz' \exp(iw_3 z') \mathbf{P}(\Omega, \mathbf{K}; z') \right], \end{aligned} \quad (29)$$

which is expressed as a sum over polarization states $\hat{q} = \{\hat{s}, \hat{p}\}$ in medium i , where $\hat{s}_+ = \hat{s}_- \equiv \hat{s}$. The Fabry-Perot term for \hat{s} and \hat{p} polarizations is

$$\mathcal{C}^q = \frac{t_{31}^q}{1 - r_{32}^q r_{31}^q \exp(i2w_3 D)}, \quad (30)$$

where t_{ij}^q and r_{ij}^q are the Fresnel coefficients for that polarization. At any point, one obtains the full electric field in space and time by applying a Fourier transform back into real time t and real space \mathbf{r} . The full broadband field can be written explicitly from Eq. (1), and its explicit calculation for different geometries and sources is the object of Section 5.

Expressions for the calculation of the radiation profile by use of Eq. (1) together with Eq. (27) and the appropriate Green function can be simplified when what is wanted is the temporal profile far from the polarization source $\mathbf{P}(\Omega, \mathbf{K}; z)$. To that end it is useful to rewrite expansions of the form of Eq. (1) involving $\mathbf{E}_+(\Omega, \mathbf{K}; z)$ as

$$\begin{aligned} \mathcal{E}(\mathbf{r}, t) &= \int_0^\infty \frac{d\Omega}{2\pi} \int \frac{id\mathbf{K}}{2\pi w} \mathbf{e}_+(\Omega, \mathbf{K}) \exp(iwz) \\ &\times \exp(i\mathbf{K} \cdot \mathbf{R} - i\Omega t) + \text{c.c.}, \end{aligned} \quad (31)$$

where

$$\mathbf{e}_+(\Omega, \mathbf{K}) \exp(iwz) = -\frac{iw}{2\pi} \mathbf{E}_+(\Omega, \mathbf{K}; z). \quad (32)$$

The far-field limit, as $r \rightarrow \infty$ with $z > 0$ and $\hat{r} = \mathbf{r}/r$ fixed, is¹⁹

$$\mathcal{E}(\mathbf{r}, t) \sim \int_0^\infty \frac{d\Omega}{2\pi} \mathbf{e}_+(\Omega, \bar{\mathbf{K}}) \frac{\exp(i\tilde{\Omega}nr - i\Omega t)}{r} + \text{c.c.}, \quad (33)$$

where the values of w and n are calculated in the medium where the wave is propagating in the far field and $\bar{\mathbf{K}} = \nu\hat{r} \cdot (\bar{\mathbf{U}} - \hat{z}\hat{z})$, where $\bar{\mathbf{U}}$ is the unit tensor. Clearly, the Fourier component with wave vector $\bar{\mathbf{K}}$ dominates for a given \hat{r} and frequency Ω . For instance, if one looks at the beam at a far distance z in the direction of the \hat{z} axis, then $\hat{r} = \hat{z}$ and $\bar{\mathbf{K}} = \nu\hat{z} \cdot (\bar{\mathbf{U}} - \hat{z}\hat{z}) = \mathbf{0}$.

5. EXAMPLE CALCULATIONS

We first discuss how to use Eq. (1) to calculate the temporal profile for an infinite medium. The integral over Ω is

a simple Fourier transform, but the integral over \mathbf{K} in Eq. (1) is complicated because of the vector nature of \mathbf{K} . The product $\mathbf{K} \cdot \mathbf{R}$, the arbitrary distribution $\mathbf{P}(\Omega, \mathbf{K}; z)$, and the implicit dependence of \hat{s} and \hat{p}_\pm on \mathbf{K} [Eqs. (8) and (9)] make the integral over the orientation of \mathbf{K} nontrivial, except for the far-field case, for which expression (33) can be used. Moreover, in general, radiated field $\mathcal{E}(\mathbf{r}, t)$ has components along all three Cartesian coordinates even if $\mathbf{P}(\Omega, \mathbf{K}; z)$ is linearly polarized. Therefore, before explicitly integrating Eq. (1) it is useful to make appropriate assumptions about the polarization source $\mathbf{P}(\Omega, \mathbf{K}; z)$, as well as to restrict ourselves to the component of interest of the radiated field.

To illustrate the use of the formalism, we calculate the temporal profile of the electric-field component polarized along \hat{x} , at $R = 0$ (i.e., on the \hat{z} axis) for the upward-propagating wave originating from polarization source $\mathcal{P}(\mathbf{r}, t)$. Also, we take polarization source $\mathcal{P}(\mathbf{r}, t)$ to be cylindrically symmetric and linearly polarized along \hat{x} , thereby making it simple to describe the polarization density and easy to evaluate the integrals. These approximations correspond to most experimental situations in the literature today and illustrate all features of the formalism.

To illustrate the results with an analytically simple case, we first consider a cylindrically symmetric sheet of polarization

$$\mathbf{P}(\Omega, \mathbf{K}; z) = \hat{x}P(\Omega, K)\delta(z) \quad (34)$$

embedded in a uniform medium of index of refraction n_1 .

A. Asymptotic Expression for the Far Field

A simple expression for the far-field temporal profile from the polarization sheet [Eq. (34)] can be obtained by use of the Green function [Eq. (28)] for an infinite medium in the general expression for the field [Eq. (27)] and by substitution of the field in the far-field limit [expression (33)]. For an observation point on the \hat{z} axis (i.e., $\mathbf{r} = z\hat{z}$ and therefore $\bar{\mathbf{K}} = \mathbf{0}$), the \hat{x} component of the field is given by

$$\begin{aligned} \hat{x} \cdot \mathcal{E}(z\hat{z}, t) &\sim \frac{1}{4\pi\epsilon_3 z} \int_0^\infty \frac{d\Omega}{2\pi} \tilde{\Omega}^2 P(\Omega, 0) \\ &\times \exp(i\tilde{\Omega}n_1 z - i\Omega t) + \text{c.c.} \end{aligned} \quad (35)$$

The results for polarization with a Gaussian spectrum and a Gaussian spatial profile,

$$P(\Omega, K) = \frac{4\pi^{3/2}}{\sigma_\Omega \sigma_K^2} P_o \exp(-\Omega^2/\sigma_\Omega^2) \exp(-K^2/\sigma_K^2), \quad (36)$$

are shown in Fig. 4 for $z = 50$ mm in local time $t' = t - z \text{Re}(n_1)/c$, where $\text{Re}(n_1)$ is the real part of the index of refraction and P_o is the peak polarization density. The far-field profile follows the time derivative of the current, $\partial\mathcal{I}/\partial t = \partial^2\mathcal{P}/\partial t^2$, as can be seen from the figure. Alternatively, it can be seen directly from expression (35), as the temporal Fourier transform of the time derivative of the current is proportional to $\Omega^2 P(\Omega, K)$.

B. Near and Far Fields

In general, the detector must be sufficiently far from the source for the asymptotic limit [expression (35)] to be adequate. If such is not the case, one must integrate Eq. (1). The integral over \mathbf{K} is written out as a two-dimensional integral in cylindrical coordinates, where $K = |\mathbf{K}|$ and ϕ is the angle between the \hat{x} axis and vector \mathbf{K} . All dyadics of the form $\hat{a}\hat{b}$, where \hat{a} and \hat{b} are \hat{s} or one value of \hat{p} , are expanded in the form

$$\hat{a}\hat{b} = \sum_m \vec{f}_m(\hat{a}\hat{b})\exp(-im\phi), \quad (37)$$

where only a finite number of coefficients $\vec{f}_m(\hat{a}\hat{b})$ survive ($m = \pm 2, \pm 1, 0$). These coefficients are easily determined and are given in Appendix A. The integral over ϕ can then be performed analytically, whereas the remaining integrals over Ω and K are performed numerically. Performing one of the integrals analytically considerably reduces both the computing time and the memory requirements for the remaining computation and makes the results developed here easily handled by a modest personal computer.

To obtain the x component of the upward-propagating field in the case of a polarization sheet [Eq. (34)] in an infinite medium, Eqs. (27) and (28) are used:

$$\begin{aligned} \hat{x} \cdot \mathbf{E}_+(\Omega, \mathbf{K}; z) = & \frac{i\tilde{\Omega}^2}{2\epsilon_0 w_1} \left\{ \sum_m [\vec{f}_m(\hat{s}\hat{s}) \right. \\ & \left. + \vec{f}_m(\hat{p}_{1+}\hat{p}_{1+})] \exp(-im\phi) \right\} \\ & \cdot \hat{x} \exp(iw_1 z) P(\Omega, K). \end{aligned} \quad (38)$$

The \hat{x} component of $\mathbf{E}_+(\Omega, \mathbf{K}; z)$ follows from the use of \vec{f}_m given in Appendix A:

$$\begin{aligned} \hat{x} \cdot \mathbf{E}_+(\Omega, \mathbf{K}; z) = & \frac{i\tilde{\Omega}^2}{2\epsilon_0 w_1} \left(\frac{1}{2} - \frac{1}{2} \cos 2\phi + \frac{w_1^2}{2\nu_1^2} \right. \\ & \left. + \frac{w_1^2}{2\nu_1^2} \cos 2\phi \right) \exp(iw_1 z) P(\Omega, K). \end{aligned} \quad (39)$$

To obtain the temporal profile of the THz field we substitute Eq. (39) into Eq. (1) and integrate over ϕ , Ω , and K ;

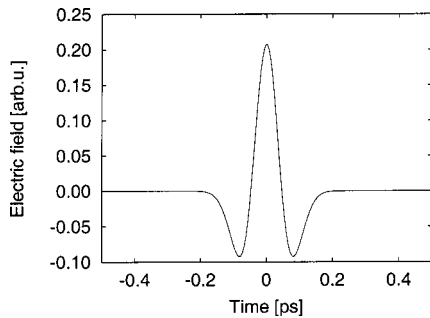


Fig. 4. Temporal profile showing the far field at $z = 50$ mm for $2\pi\sigma_\Omega^{-1} = 200$ fs and $2\pi\sigma_K^{-1} = 1$ mm in a medium with $n_1^2 = 10 + i10^{-4}$, similar to dispersionless GaAs. The field follows the second time derivative of the polarization envelope function.

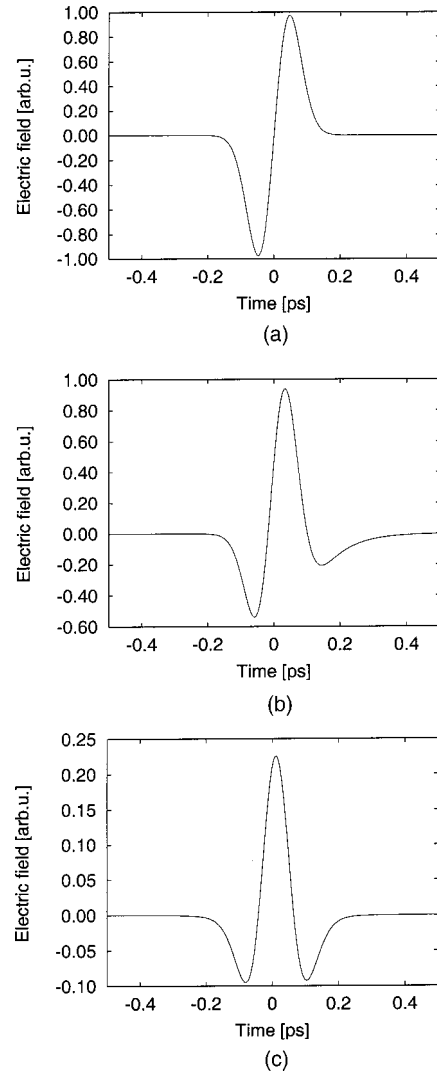


Fig. 5. Temporal profiles showing the transitions from near to far field for common THz parameters with $2\pi\sigma_\Omega^{-1} = 200$ fs and $2\pi\sigma_K^{-1} = 1$ mm in a medium with a dielectric constant $n_1^2 = 10 + i10^{-4}$ similar to dispersionless GaAs. (a) $z = 0$ mm, (b) $z = 8$ mm, (c) $z = 50$ mm. The arbitrary units are the same for all three figures and are the same as those used in Fig. 4.

the first integral is done analytically. For an observation point at $\mathbf{r} = z\hat{z}$ (i.e., on axis), we obtain

$$\begin{aligned} \hat{x} \cdot \mathcal{E}(z\hat{z}, t) = & \frac{i}{2\epsilon_0} \int_0^\infty \frac{d\Omega}{2\pi} \tilde{\Omega}^2 \exp(-i\Omega t) \int_0^\infty \frac{KdK}{2\pi} \\ & \times \left(\frac{1}{2} + \frac{w_1^2}{2\nu_1^2} \right) w_1^{-1} \exp(iw_1 z) P(\Omega, K). \end{aligned} \quad (40)$$

When a broad range of wave vectors \mathbf{K} is present, w_1 can decrease to a small value or even become imaginary. If n_1 is real, divergence w_1^{-1} is purely formal because it can be integrated over and can easily be handled analytically. In practice, however, any residual absorption in medium 1 will ensure that w_1 never vanishes [Eq. (7)]. The integrand is then strongly peaked but can be integrated numerically with appropriate sampling. The integrand is sampled at different values of $K[i]$ where

$w_1(\Omega, K[i+1]) - w_1(\Omega, K[i])$ is constant and equal to Δ , as long as the corresponding change in $K[i+1] - K[i]$ is smaller than Δ . Sampling parameter Δ is decreased appropriately until the calculated results do not change. Results for a polarization of the type of Eq. (36) are shown in Fig. 5 in local time $t' = t - z \text{Re}(n_1)/c$ and at several z values. We see the onset of the asymptotic solution [expression (35)] as the distance from the source is increased. The radiated field follows the current or the time derivative of the polarization $\mathcal{J} = \partial\mathcal{P}/\partial t$ close to the source but is reshaped into the time derivative of the current density $\partial\mathcal{J}/\partial t = \partial^2\mathcal{P}/\partial t^2$ in the far field, as was obtained for Fig. 4.

6. EXPERIMENTAL GEOMETRIES AND SOURCES

To extend the previous results to experimentally interesting geometries and polarization sources is straightforward. The geometry of Fig. 3, often encountered in experiments, is considered. For the purpose of example, we consider a linearly polarized, cylindrically symmetric, optically generated polarization source, as obtained from below bandgap second-order rectification.^{6,14,20} The source substrate of thickness $D = 100 \mu\text{m}$ is (110)-oriented GaAs and is surrounded by air (i.e., $n_1 = n_2 = 1$), as shown in Fig. 3. The only nonzero second-order susceptibility coefficients of GaAs are $\chi_2^{(xyz)} = 100 \text{ pm V}^{-1}$, where (xyz) is any permutation of xyz . The frequency-dependent index of refraction $n_3(\Omega)$ of GaAs is obtained from experimental data.²¹ The optical pump beam is assumed to be normally incident from $z < -D$ upon the GaAs (medium 3). The spectrum of an optical pump beam centered at ω_0 with a Gaussian spatial profile is described [Eq. (3)] by

$$E_+(\omega, \mathbf{K}) \exp(-i\omega_0 D/c) = \frac{4\pi^{3/2}}{\sigma_{\omega_0} \sigma_{\kappa_0}^2} E_{\omega_0} \exp[-(\omega - \omega_0)^2/\sigma_{\omega_0}^2] \times \exp(-|\mathbf{K}|^2/\sigma_{\kappa_0}^2), \quad (41)$$

with a positive center frequency $2\pi c \omega_0^{-1} = 1.55 \mu\text{m}$, a spectral width $2\sigma_{\omega_0}^{-1} = 125 \text{ fs}$, and a spot $1/e$ width $100 \mu\text{m}$, giving $2\sigma_{\kappa_0}^{-1} = 100 \mu\text{m}$ with a peak intensity inside the crystal of $2|E_{\omega_0}|^2 n_3/Z_0 = 5 \text{ GW cm}^{-2}$, where $Z_0 = 377 \Omega$ is the vacuum impedance. Neglecting diffraction of the optical pump beam yields the following polarization density $\mathbf{P}(\Omega, \mathbf{K}; z)$:

$$\mathbf{P}(\Omega, \mathbf{K}; z) = \hat{x}P(\Omega, K) \exp[(in_{\omega_0}^g \tilde{\Omega} - 2\alpha_{\omega_0})(z + D)], \quad (42)$$

with

$$P(\Omega, K) = 2\epsilon_0 \chi_2^{\text{eff}} |E_{\omega_0}|^2 \frac{4\pi^{3/2}}{\sigma_{\omega_0} \sigma_{\kappa_0}^2} \exp(-\Omega^2/\sigma_{\Omega}^2) \times \exp(-K^2/\sigma_K^2). \quad (43)$$

Here $\chi_2^{\text{eff}} = \chi_2^{(xyz)}/2$ is the effective nonlinear susceptibility with the optical pump fields polarized along \hat{y} ($\hat{1}10$); σ_{Ω}

$= \sqrt{2}\sigma_{\omega_0}$ and $\sigma_K = \sqrt{2}\sigma_{\kappa_0}$ are the spectral widths in frequency space Ω and transverse wave-vector space \mathbf{K} , respectively; $n_{\omega_0}^g = 3.1$ is the pump's group index; and α_{ω_0} is the field absorption coefficient at pump frequency ω_0 .

A. Asymptotic Expression for the Far Field

To obtain the far-field radiation propagating in the positive \hat{z} direction in the medium 1, we substitute polarization equation (42) into the expression for the field [Eq. (29)] and use the result in Eq. (32) to obtain

$$\begin{aligned} \mathbf{e}_+(\Omega, \mathbf{K}) = & \frac{\tilde{\Omega}^2}{4\pi\epsilon_0} \sum_{\hat{q}} C^q \left[\hat{q}_{3+} \cdot \int_{-D}^0 dz' \right. \\ & \times \exp(-iw_3 z') \mathbf{P}(\Omega, \mathbf{K}; z') \\ & + r_{32}^q \exp(2iw_3 D) \hat{q}_{3-} \cdot \int_{-D}^0 dz' \\ & \left. \times \exp(iw_3 z') \mathbf{P}(\Omega, \mathbf{K}; z') \right], \quad (44) \end{aligned}$$

which we substitute into the general expression for the far field [expression (33)]. The integral over z' can be performed analytically and written as

$$\begin{aligned} \int dz' \exp(\mp iw_3 z') \mathbf{P}(\Omega, \mathbf{K}; z') \\ = \hat{x}P(\Omega, K) \int_{-D}^0 dz' \exp[(in_{\omega_0}^g \tilde{\Omega} - 2\alpha_{\omega_0}) \\ \times (z + D)] \exp(\mp iw_3 z') \quad (45) \end{aligned}$$

$$\equiv \hat{x}P(\Omega, K) L_{\pm}(\Omega, K), \quad (46)$$

where $L_{\pm}(\Omega, K)$ is the effective interaction length for the upward- and downward-propagating waves,

$$L_{\pm}(\Omega, K) = \left[\frac{\exp(in_{\omega_0}^g \tilde{\Omega} D - 2\alpha_{\omega_0} D) - \exp(\pm iw_3 D)}{\mp iw_3 + in_{\omega_0}^g \tilde{\Omega} - 2\alpha_{\omega_0}} \right], \quad (47)$$

and grows in magnitude as the fields approach the usual phase-matching condition. For an observation point on the \hat{z} axis (i.e., $\mathbf{r} = z\hat{z}$ and therefore $\tilde{\mathbf{K}} = \mathbf{0}$), the \hat{x} component of the temporal profile of the beam is

$$\begin{aligned} \hat{x} \cdot \mathcal{E}(z\hat{z}, t) \sim & \int \frac{d\Omega}{2\pi} \frac{\tilde{\Omega}^2}{4\pi\epsilon_0} C^s P(\Omega, 0) [L_+(\Omega, 0) \\ & + r_{32}^s \exp(2iw_3 D) L_-(\Omega, 0)] \\ & \times \frac{\exp(i\tilde{\Omega}nz - i\Omega t)}{z} + \text{c.c.}, \quad (48) \end{aligned}$$

where we took $\hat{x} \cdot \hat{s} = 1$ and $\hat{x} \cdot \hat{p} = 0$ to lift the ambiguity of Eqs. (8) and (9) at $\tilde{\mathbf{K}} = \mathbf{0}$. The results are shown in Fig. 6 at $z = 5 \text{ cm}$ for the polarization source described by Eq. (42), with the same parameters as before except for a larger bandwidth, $\sigma_{\Omega}/2\pi = 3.8 \text{ THz}$. The spectrum of this radiation slightly overlaps the first phonon resonance at 8.5 THz in GaAs, which is implicitly included by means of $n_3(\Omega)$. Our results demonstrate how all the disper-

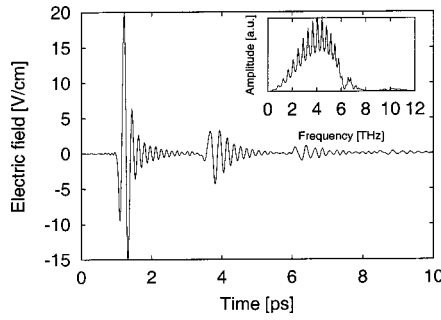


Fig. 6. Temporal profile of THz radiation from below bandgap optical rectification with $\sigma_{\Omega}/2\pi = 3.8$ THz at $z = 5$ cm. Inset, spectrum amplitude.

sive features of the source material are included in the calculation. The inset of Fig. 6 shows the corresponding spectrum amplitude; one can clearly see Fabry-Perot and phonon resonances as well as the effects of the frequency-dependent interaction length (which is zero at 6.1 THz).

B. Near and Far Fields

An approach similar to that which was used in Section 5 to calculate the near field for the polarization sheet is used here to calculate the near-field temporal profile. Starting from Eq. (29), the \hat{x} component of the field from both polarizations is

$$\begin{aligned} \hat{x} \cdot \mathbf{E}_+(\Omega, \mathbf{K}; z) &= \frac{i\tilde{\Omega}^2}{2\epsilon_0 w_3} \exp(iw_1 z) \\ &\times \sum_{\hat{q}} C^q \left[\int_{-D}^0 dz' \exp(-iw_3 z') \hat{x} \cdot \hat{q}_{1+\hat{q}_{3+}} \right. \\ &\cdot \hat{x} P(\Omega, \mathbf{K}; z') + r_{32}^q \exp(2iw_3 D) \int_{-D}^0 dz' \\ &\left. \times \exp(iw_3 z') \hat{z} \cdot \hat{q}_{1+\hat{q}_{3-}} \cdot \hat{x} P(\Omega, \mathbf{K}'; z') \right]. \quad (49) \end{aligned}$$

Using the results of Appendix A, we rewrite $\hat{x} \cdot \hat{q}_{1+\hat{q}_{3+}} \cdot \hat{x}$ and $\hat{x} \cdot \hat{q}_{1+\hat{q}_{3-}} \cdot \hat{x}$ and obtain the equation for the field:

$$\begin{aligned} \hat{x} \cdot \mathbf{E}_+(\Omega, \mathbf{K}; z) &= \frac{i\tilde{\Omega}^2}{2\epsilon_0 w_3} \exp(iw_1 z) P(\Omega, K) \left[L_+(\Omega, K) \right. \\ &\times \left(\frac{1}{2} C^s - \frac{1}{2} C^s \cos 2\phi + \frac{w_1 w_3}{2\nu_1 \nu_3} C^p \right. \\ &\left. + \frac{w_1 w_3}{2\nu_1 \nu_3} C^p \cos 2\phi \right) \\ &\left. + \exp(2iw_3 D) L_-(\Omega, K) \left(\frac{1}{2} r_{32}^s C^s \right. \right. \\ &\left. - \frac{1}{2} r_{32}^s C^s \cos 2\phi - \frac{w_1 w_3}{2\nu_1 \nu_3} r_{32}^p C^p \right. \\ &\left. \left. - \frac{w_1 w_3}{2\nu_1 \nu_3} r_{32}^p C^p \cos 2\phi \right) \right]. \quad (50) \end{aligned}$$

Finally, to obtain the total field, we integrate Eq. (1) over Ω and \mathbf{K} with Eq. (50). The integral over ϕ , the orientation of \mathbf{K} , is performed analytically, leaving us with

$$\begin{aligned} \hat{x} \cdot \mathcal{E}(z\hat{z}, t) &= \int_0^\infty \frac{d\Omega}{2\pi} \exp(-i\Omega t) \frac{i\tilde{\Omega}^2}{2\epsilon_0} \\ &\times \int_0^\infty \frac{K dK}{2\pi} w_3^{-1} \exp(iw_1 z) P(\Omega, K) \\ &\times \left[\left(\frac{1}{2} C^s + \frac{w_1 w_3}{2\nu_1 \nu_3} C^p \right) L_+(\Omega, K) \right. \\ &\left. + \exp(2iw_3 D) \left(\frac{1}{2} C^s r_{32}^s \right. \right. \\ &\left. \left. - \frac{w_1 w_3}{2\nu_1 \nu_3} C^p r_{32}^p \right) L_-(\Omega, K) \right] + \text{c.c.} \quad (51) \end{aligned}$$

to integrate numerically. The integrand is strongly peaked as w_3 approaches zero, and sampling of the function is done at different points $K[i]$ that correspond to a constant separation in w_3 , as explained above. The on-axis temporal profile of the THz radiation from below-bandgap optical rectification from a 100- μm substrate of GaAs is shown in Fig. 7. Multiple pulse reflections separated by 2.3 ps (as expected from the thickness of the substrate and its group index at THz frequencies) are observed. The pulses that arise from the multiple reflections are increasingly chirped because of the dispersion of GaAs and the fact that the reflected pulses have traveled repeatedly through the sample.

C. Gaussian Beam through a Finite-Sized Lens

We have shown in the previous sections how to calculate the near- and far-field temporal profiles of a THz beam as it propagates exclusively through layered media. However, because experimental THz radiation sources are often essentially point sources, diffraction is important, and the THz radiation must be collimated with optics for experiments. The dimensions of the optics are such that their finite clear apertures cannot collect all the energy of low frequencies of the THz spectrum that have diffracted to a size larger than the diameter of the collimating optics. Various experimental designs make use of off-axis parabolic mirrors (with a typical diameter of 2.5 cm) to collimate and focus THz beams. Their finite size has the

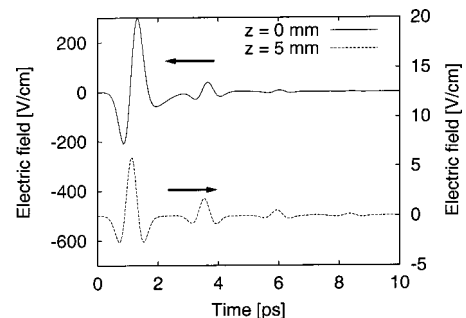


Fig. 7. Temporal profile of THz radiation from below bandgap optical rectification with $\sigma_{\Omega}/2\pi = 1$ THz near and far from the source.

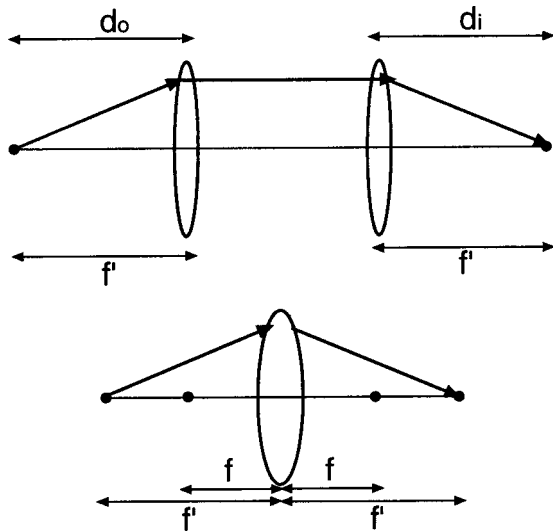


Fig. 8. Two lenses of focal length f' used to collimate and refocus a point source located at the focus of one of the lenses are equivalent to a single lens with a focal length twice as short, $f = f'/2$; d_o (d_i), distance between object (image) plane and lens.

effect of filtering out low frequencies while letting through the higher frequencies. Also, most THz detection systems make use of a pair of matched mirrors with focal length f' , set up far from the source and in such a way that the first one collimates a THz point source and the second one focuses it. Within the usual approximations,¹⁷ this arrangement can be treated as a single optical element of focal length $f = f'/2$, with $d_o = d_i = f'$ (see Fig. 8). We assume that these mirrors are adequately modeled by finite-sized thin lenses, as is usually assumed in optics,¹⁷ and it is therefore sufficient to study the case of a beam going through a single lens replacing the mirrors. The transformation of an arbitrary beam by the mirrors is then given by that of the lens in Eq. (25). In this section we make an example calculation, using the results of Subsection 3.B for the effect of finite-sized mirrors on the spectrum and the temporal profile of THz beams. In general, the results of the transformation depend on the spatial profile and on the radius of curvature of the beam at the entrance of the lens and is an imaging problem beyond the scope of the study reported here. Therefore we make the simplifying assumption that the input spatial profile is Gaussian, as is often the case experimentally.

We start with a linearly polarized Gaussian beam $\mathbf{E}_+(\Omega, \mathbf{K}) = 4\pi\sigma_K^{-2}\mathbf{E}_+(\Omega)\exp(-K^2/\sigma_K^2)$ at $z = 0$, where σ_K is the (real) Gaussian width of the transverse wave-vector distribution and $\mathbf{E}_+(\Omega) = \hat{x}E_+(\Omega)$ an arbitrary spectral density. At a distance d_o from its waist is a lens of focal length $f = R_0/(n - 1)$, and we are interested in calculating the field at a distance d_i behind the lens (see Fig. 9). Using the paraxial wave approximation,²² we can write the field immediately in front of the lens as

$$\mathbf{E}_+(\Omega, \mathbf{K}; d_o^-) = \mathbf{E}_+(\Omega, \mathbf{K})\exp\left(i\tilde{\Omega}d_o - i\frac{K^2d_o}{2\tilde{\Omega}}\right). \tag{52}$$

A Gaussian spatial profile can therefore be written as

$$\mathbf{E}_+(\Omega, \mathbf{K}; d_o^-) = \frac{4\pi}{\sigma_K^2}\mathbf{E}_+(\Omega)\exp(i\tilde{\Omega}d_o)\exp\left(-\frac{K^2}{\sigma_i^2(d_o)}\right), \tag{53}$$

with

$$\frac{1}{\sigma_o^2(d_o)} = \frac{1}{\sigma_K^2} + i\frac{d_o}{2\tilde{\Omega}}. \tag{54}$$

The lens transformation of Eq. (25) is performed with an input wave distribution of the form of Eq. (53) with the help of identities (23) and (24). We obtain the field immediately behind the lens with

$$\begin{aligned} \mathbf{E}_+(\Omega, \mathbf{K}; d_o^+) &= \frac{4\pi}{\sigma_K^2} \frac{\sigma_o^2(d_o)}{\sigma_o^2(d_o) + iK_L^2} \mathbf{E}_+(\Omega) \\ &\times \exp(i\tilde{\Omega}d_o)\exp\left[-\frac{K^2}{\sigma_o^2(d_o) + iK_L^2}\right]. \end{aligned} \tag{55}$$

The field after a propagation by a distance d_i is then obtained simply by multiplying Eq. (55) by $\exp(i\tilde{\Omega}d_i)$ [see Eq. (11)]:

$$\begin{aligned} \mathbf{E}_+(\Omega, \mathbf{K}; d_o + d_i) &= \frac{4\pi}{\sigma_K^2} \frac{\sigma_o^2(d_o)}{\sigma_i^2(d_o, 0)} \mathbf{E}_+(\Omega)\exp[i\tilde{\Omega}(d_o \\ &+ d_i)]\exp\left[-\frac{K^2}{\sigma_i^2(d_o, d_i)}\right], \end{aligned} \tag{56}$$

where we have defined for simplicity

$$\frac{1}{\sigma_i^2(d_o, d_i)} = \frac{1}{\sigma_o^2(d_o) + iK_L^2} + \frac{id_i}{2\tilde{\Omega}}. \tag{57}$$

When the total field is calculated, for instance with Eq. (1), on the z axis (i.e., $\mathbf{R} = 0$), and with polarization \hat{x} , the relative attenuation of frequency component Ω of the field at $z = d_o + d_i$ compared to the field at $z = 0$ is given by

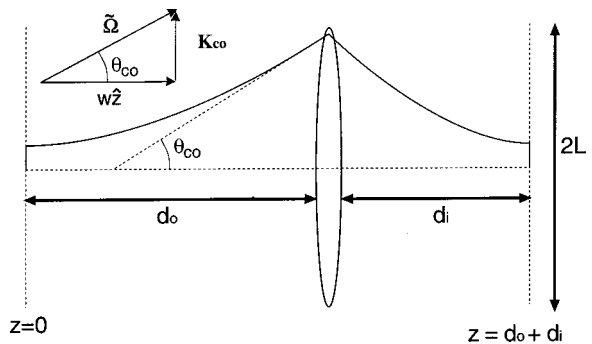


Fig. 9. Diffraction of a Gaussian beam originating from $z = 0$ and transformation by a lens at $z = d_o$. The field at $z = d_o + d_i$ is obtained. Inset, estimation of the cutoff frequency when the lens is far from a point source with $\tan \theta_{co} = L/d_o \approx |\mathbf{K}_{co}|/\tilde{\Omega}$.

$$\begin{aligned} \mathcal{F}^{\text{full}}(\Omega, d_o, d_i) &= \frac{\hat{x} \cdot \int [\mathbf{d}\mathbf{K}/(2\pi)^2] \mathbf{E}_+(\Omega, \mathbf{K}; d_o + d_i)}{\hat{x} \cdot \int [\mathbf{d}\mathbf{K}/(2\pi)^2] \mathbf{E}_+(\Omega, \mathbf{K}; 0)} \\ &= \frac{\sigma_o^2(d_o) \sigma_i^2(d_o, d_i)}{\sigma_o^2(0) \sigma_i^2(d_o, 0)}, \end{aligned} \quad (58)$$

and its magnitude is shown in Fig. 10 for $\sigma_K^{-1} = 100 \mu\text{m}$, $L = 2.5 \text{ cm}$, $f = 2.5 \text{ cm}$, and $d_o = d_i = 5 \text{ cm}$, corresponding to typical THz parameters. The lens acts as a low-frequency filter. Low frequencies diffract more than do high frequencies and, therefore, their Gaussian spatial profiles at the lens are wider than the lens itself and do not get fully collimated. Higher frequencies, however, do not diffract so much and are almost entirely collimated. This result is entirely expected and can be understood intuitively with the following physical argument: From previous results we know that the far field in a given direction is related to a single transverse wave vector \mathbf{K} . Therefore the finite clear aperture of the lens can be seen as collimating all waves that make an angle with the \hat{z} axis smaller than θ_{co} , with $\tan \theta_{\text{co}} = L/d_o \approx |\mathbf{K}_{\text{co}}|/\tilde{\Omega}$ (Fig. 9). Therefore any plane-wave component $\mathbf{E}_+(\Omega, \mathbf{K})$ with $|\mathbf{K}| < |\mathbf{K}_{\text{co}}|$ goes through the collimating lens, whereas a component with $|\mathbf{K}| > |\mathbf{K}_{\text{co}}|$ does not. Inasmuch as we are assuming a Gaussian spatial profile, the filter function can be approximated by

$$\mathcal{F}^{\text{approx}}(\Omega) = \text{erf}^2\left(\frac{\tilde{\Omega}L}{f\sigma_K}\right), \quad (59)$$

which is also plotted in Fig. 10 for $\sigma_K^{-1} = 100 \mu\text{m}$, $L = 2.5 \text{ cm}$, $f = 2.5 \text{ cm}$, and $d_o = d_i = 5 \text{ cm}$. The effect of a collimating lens placed in the far field is therefore to limit the contribution to the profile of transverse wave vectors $|\mathbf{K}| < L\tilde{\Omega}/f$. The beam after collimation and focusing can be obtained from

$$\begin{aligned} \mathbf{E}_+(\Omega, \mathbf{K}; d_o + d_i) &= \mathbf{E}_+(\Omega, \mathbf{K}; d_o^-) \mathcal{F}^{\text{approx}}(\Omega) \\ &\times \exp\left(i \frac{2fK^2}{\tilde{\Omega}}\right) \exp(i\omega d_i). \end{aligned} \quad (60)$$

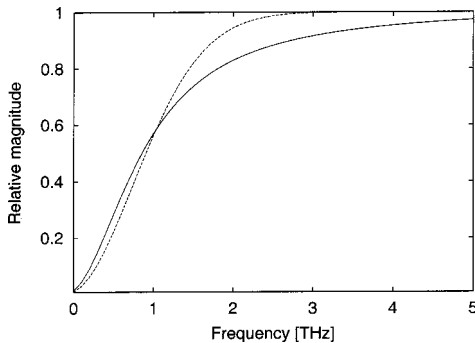


Fig. 10. Magnitude of filter functions $\mathcal{F}^{\text{full}}$ (solid curve) and $\mathcal{F}^{\text{approx}}$ (dotted curve) for $\sigma_K^{-1} = 100 \mu\text{m}$, $L = 2.5 \text{ cm}$, $f = 2.5 \text{ cm}$, and $d_o = d_i = 5 \text{ cm}$.

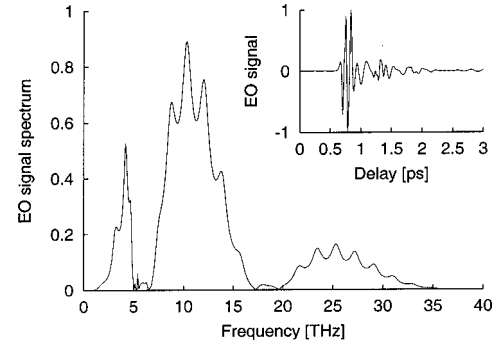


Fig. 11. Calculation in a $30\text{-}\mu\text{m}$ ZnTe crystal of the temporal profile and spectrum of THz radiation from below bandgap optical rectification detected in a $27\text{-}\mu\text{m}$ -thick ZnTe crystal. These calculations agree well with published results.²³ EO, electro-optic.

The filter function $\mathcal{F}^{\text{approx}}(\Omega)$ is for the finite size effect of the mirror, $\exp[i(2fK^2/\tilde{\Omega})]$ is the phase curvature introduced by an infinite lens with a focal length equivalent to that of the pair of matched mirrors, and $\exp(i\omega d_i)$ is a propagation factor from the lens to the focal plane. At $\Omega = 0$, the limit of Eq. (60) is zero. Experimental results of THz radiation that is collimated and refocused can be modeled well with the combined use of near-field expressions and filtering functions from collimating, focusing, and propagating the beam. For example, the calculation of THz radiation from optical rectification in a $30\text{-}\mu\text{m}$ ZnTe crystal detected in a $27\text{-}\mu\text{m}$ ZnTe crystal (similar to the experimental results reported by Han and Zhang²³) is shown in Fig. 11. The calculation makes use of Eq. (50) with the additional multiplication by filter function Eq. (60). The detection by means of electro-optic sampling has been described elsewhere²⁴ and is an additional filter function. The full dispersion curve of ZnTe was obtained from Leitenstorfer *et al.*²⁵ and is used in calculation of the index of refraction $n_3(\Omega)$ at THz frequency as well as for the electro-optic detection filter function. These calculations agree well with published results.²³ The exact temporal profile is strongly dependent on the frequency-dependent index of ZnTe, and small temporal features are not easily reproduced when strong phonon resonances are present, as is the case here.

7. CONCLUSIONS

Plane waves with polarization bases \hat{s} and \hat{p} are ideal for describing the linear propagation of electromagnetic radiation because these two polarizations can be treated independently, even in the presence of layered structures. In an infinite medium the Green function that relates the radiated field to the source is known and the radiated electric field is obtained by integration over all plane waves of all frequencies and directions. In the far field it is possible to simplify these integrals greatly, because only the plane waves that have wave vectors in the direction of the observation point contribute to the field. In the near field it is possible to simplify the expressions for the field if one makes the usual assumptions that are easily met in practice, such as linear polarization and Gaussian spatial profiles. The remaining integrals are then easily implemented numerically. The generality of the

method and its applicability to experimental situations is demonstrated when thin-film transfer matrices are used in conjunction with the boundary conditions (i.e., incoming and outgoing waves) to produce the Green function for a polarization embedded in a three-layer structure. We used this Green function to calculate the temporal profiles of the far and near-field radiation for a spatially Gaussian polarization source [Eqs. (44) and (51)] and included the dispersion of the source material, the multiple reflections in the material, and the polarization dependence of the transmissions and reflections at interfaces. Finally, a pair of mirrors, often encountered experimentally for collimating and refocusing a THz pulse, is shown to cut off low frequencies but to let higher frequencies through mostly unaltered. The cutoff frequency depends on the focal length, the size of the mirror, and the size of the THz source. A complete modeling of experiments is possible when the details of the frequency response of the THz detection system are known. The dispersive properties of various THz measurement schemes have been studied and compared elsewhere.^{8,24–26} One example of experimental data from the literature²³ has been shown to be well modeled by the formalism presented in this paper. The straightforward application to experimental situations of the model presented here allows one to extract details about the THz generation process, as has been demonstrated elsewhere.¹⁴ A computer implementation of the results for calculating the various THz temporal profiles presented in the present paper is available on line.²⁷

APPENDIX A: ANGULAR EXPANSION OF THE POLARIZATION TENSORS

The various Fourier decompositions $\sum_m \vec{f}_m \exp(-im\phi)$ of the polarization tensors are calculated. For each frequency Ω and transverse wave vector \mathbf{K} , \hat{s} and $\hat{p}_{i\pm}$ polarization vectors as well as \hat{K} are defined in medium i as

$$\hat{K} = \hat{x} \cos \phi + \hat{y} \sin \phi,$$

$$\hat{s} = \hat{K} \times \hat{z} = -\hat{y} \cos \phi + \hat{x} \sin \phi,$$

$$\begin{aligned} \hat{p}_{i\pm} &= \frac{1}{\nu_i} (K\hat{z} \mp w_i \hat{K}) \\ &= \frac{K}{\nu_i} \hat{z} \mp \frac{w_i}{\nu_i} \hat{x} \cos \phi \mp \frac{w_i}{\nu_i} \hat{y} \sin \phi. \end{aligned}$$

Nonvanishing $\vec{f}_m(\hat{s}\hat{s})$

$$\vec{f}_0(\hat{s}\hat{s}) = \frac{1}{2}(\hat{x}\hat{x} + \hat{y}\hat{y}),$$

$$\vec{f}_{+2}(\hat{s}\hat{s}) = \frac{1}{2} \left[-\frac{1}{2}(\hat{x}\hat{x} - \hat{y}\hat{y}) \right] + \frac{i}{2} \left[-\frac{1}{2}(\hat{x}\hat{y} + \hat{y}\hat{x}) \right],$$

$$\vec{f}_{-2}(\hat{s}\hat{s}) = \frac{1}{2} \left[-\frac{1}{2}(\hat{x}\hat{x} - \hat{y}\hat{y}) \right] - \frac{i}{2} \left[-\frac{1}{2}(\hat{x}\hat{y} + \hat{y}\hat{x}) \right].$$

Nonvanishing $\vec{f}_m(\hat{p}_{\pm i}\hat{p}_{\pm j})$

$$\vec{f}_0(\hat{p}_{\pm i}\hat{p}_{\pm j}) = \frac{K^2}{\nu_i \nu_j} \hat{z}\hat{z} + \frac{w_i w_j}{2 \nu_i \nu_j} (\hat{x}\hat{x} + \hat{y}\hat{y}),$$

$$\begin{aligned} \vec{f}_{+1}(\hat{p}_{\pm i}\hat{p}_{\pm j}) &= \mp \frac{1}{2} \left(\frac{Kw_j}{\nu_i \nu_j} \hat{z}\hat{x} + \frac{Kw_i}{\nu_i \nu_j} \hat{x}\hat{z} \right) \\ &\mp \frac{i}{2} \left(\frac{Kw_j}{\nu_i \nu_j} \hat{z}\hat{y} + \frac{Kw_i}{\nu_i \nu_j} \hat{y}\hat{z} \right) \end{aligned}$$

$$\begin{aligned} \vec{f}_{-1}(\hat{p}_{\pm i}\hat{p}_{\pm j}) &= \mp \frac{1}{2} \left(\frac{Kw_j}{\nu_i \nu_j} \hat{z}\hat{x} + \frac{Kw_i}{\nu_i \nu_j} \hat{x}\hat{z} \right) \\ &\pm \frac{i}{2} \left(\frac{Kw_j}{\nu_i \nu_j} \hat{z}\hat{y} + \frac{Kw_i}{\nu_i \nu_j} \hat{y}\hat{z} \right) \end{aligned}$$

$$\begin{aligned} \vec{f}_{+2}(\hat{p}_{\pm i}\hat{p}_{\pm j}) &= \frac{1}{2} \left[\frac{w_i w_j}{2 \nu_i \nu_j} (\hat{x}\hat{x} - \hat{y}\hat{y}) \right] \\ &+ \frac{i}{2} \left[\frac{w_i w_j}{2 \nu_i \nu_j} (\hat{x}\hat{y} + \hat{y}\hat{x}) \right], \end{aligned}$$

$$\begin{aligned} \vec{f}_{-2}(\hat{p}_{\pm i}\hat{p}_{\pm j}) &= \frac{1}{2} \left[\frac{w_i w_j}{2 \nu_i \nu_j} (\hat{x}\hat{x} - \hat{y}\hat{y}) \right] \\ &- \frac{i}{2} \left[\frac{w_i w_j}{2 \nu_i \nu_j} (\hat{x}\hat{y} + \hat{y}\hat{x}) \right]. \end{aligned}$$

Nonvanishing $\vec{f}_m(\hat{p}_{\pm i}\hat{p}_{\mp j})$

$$\vec{f}_0(\hat{p}_{\pm i}\hat{p}_{\mp j}) = \frac{K^2}{\nu_i \nu_j} \hat{z}\hat{z} - \frac{w_i w_j}{2 \nu_i \nu_j} (\hat{x}\hat{x} + \hat{y}\hat{y}),$$

$$\begin{aligned} \vec{f}_{+1}(\hat{p}_{\pm i}\hat{p}_{\mp j}) &= \frac{1}{2} \left(\frac{Kw_j}{\nu_i \nu_j} \hat{z}\hat{x} \mp \frac{Kw_i}{\nu_i \nu_j} \hat{x}\hat{z} \right) \\ &+ \frac{i}{2} \left(\frac{Kw_j}{\nu_i \nu_j} \hat{z}\hat{y} \mp \frac{Kw_i}{\nu_i \nu_j} \hat{y}\hat{z} \right), \end{aligned}$$

$$\begin{aligned} \vec{f}_{-1}(\hat{p}_{\pm i}\hat{p}_{\mp j}) &= \frac{1}{2} \left(\frac{Kw_j}{\nu_i \nu_j} \hat{z}\hat{x} \mp \frac{Kw_i}{\nu_i \nu_j} \hat{x}\hat{z} \right) \\ &- \frac{i}{2} \left(\frac{Kw_j}{\nu_i \nu_j} \hat{z}\hat{y} \mp \frac{Kw_i}{\nu_i \nu_j} \hat{y}\hat{z} \right), \end{aligned}$$

$$\begin{aligned} \vec{f}_{+2}(\hat{p}_{\pm i}\hat{p}_{\mp j}) &= \frac{1}{2} \left[-\frac{w_i w_j}{2 \nu_i \nu_j} (\hat{x}\hat{x} - \hat{y}\hat{y}) \right] \\ &+ \frac{i}{2} \left[\frac{w_i w_j}{2 \nu_i \nu_j} (\hat{x}\hat{y} + \hat{y}\hat{x}) \right], \end{aligned}$$

$$\begin{aligned} \vec{f}_{-2}(\hat{p}_{\pm i}\hat{p}_{\mp j}) &= \frac{1}{2} \left[-\frac{w_i w_j}{2 \nu_i \nu_j} (\hat{x}\hat{x} - \hat{y}\hat{y}) \right] \\ &- \frac{i}{2} \left[\frac{w_i w_j}{2 \nu_i \nu_j} (\hat{x}\hat{y} + \hat{y}\hat{x}) \right]. \end{aligned}$$

ACKNOWLEDGMENTS

We thank F. Nastos and N. Laman for comments as well as Photonics Research Ontario and the Natural Sciences and Engineering Research Council of Canada for financial support.

J. E. Sipe's e-mail address is sipe@physics.utoronto.ca.

REFERENCES AND NOTES

- J. D. Jackson, *Classical Electrodynamics*, 2nd ed. (Wiley, New York, 1975), Chap. 9.
- A. E. Siegman, *Lasers* (University Science, Mill Valley, Calif., 1986), Chap. 16.
- R. Ell, U. Morgner, F. X. Kärtner, J. G. Fujimoto, E. P. Ippen, V. Scheuer, G. Angelow, T. Tschudi, M. J. Lederer, and A. B. Luther-Davies, "Generation of 5-fs pulses and octave-spanning spectra directly from a Ti:sapphire laser," *Opt. Lett.* **26**, 373–375 (2001).
- C. Fattinger and D. Grischkowsky, "Point source terahertz optics," *Appl. Phys. Lett.* **53**, 1480–1482 (1988).
- J. T. Darrow, X.-C. Zhang, and D. H. Auston, "Power scaling of large-aperture photoconducting antennas," *Appl. Phys. Lett.* **58**, 25–27 (1991).
- A. Bonvalet, M. Joffe, J. L. Martin, and A. Migus, "Generation of ultrabroadband femtosecond pulses in the mid-infrared by optical rectification of 15 fs light pulses at 100 MHz repetition rate," *Appl. Phys. Lett.* **67**, 2907–2909 (1995).
- O. Dietrich, F. Krausz, and P. B. Corkum, "Determining the absolute carrier phase of a few-cycle laser pulse," *Opt. Lett.* **25**, 16–18 (2000).
- S.-G. Park, M. R. Melloch, and A. M. Weiner, "Analysis of terahertz waveforms measured by photoconductive and electrooptic sampling," *IEEE J. Quantum Electron.* **35**, 810–819 (1999).
- E. Budiharto, N.-W. Pu, S. Jeong, and J. Bokor, "Near-field propagation of terahertz pulses from large-aperture antenna," *Opt. Lett.* **23**, 213–215 (1998).
- A. E. Kaplan, "Diffraction-induced transformation of near-cycle and subcycle pulses," *J. Opt. Soc. Am. B* **15**, 951–956 (1998).
- S. Feng, H. G. Winful, and R. W. Hellwarth, "Gouy shift and temporal reshaping of focused single-cycle electromagnetic pulses," *Opt. Lett.* **23**, 385–387 (1998); errata **23**, 1141 (1998).
- S. Hunsche, S. Feng, H. G. Winful, A. Leitenstorfer, M. C. Nuss, and E. P. Ippen, "Spatiotemporal focusing of single-cycle light pulses," *J. Opt. Soc. Am. A* **16**, 2025–2028 (1999).
- S. Nekkanti, D. Sullivan, and D. S. Citrin, "Simulation of spatiotemporal terahertz pulse shaping in 3-D using conductive apertures of finite thickness," *IEEE J. Quantum Electron.* **37**, 1226–1231 (2001).
- D. Côté, N. Laman, and H. M. van Driel, "Rectification and shift currents in GaAs," *Appl. Phys. Lett.* **80**, 905–907 (2002).
- J. E. Sipe, "New Green-function formalism for surface optics," *J. Opt. Soc. Am. B* **4**, 481–489 (1987).
- M. Born and E. Wolf, *Principles of Optics*, 6th ed. (Pergamon, New York, 1985), Chap. 1, p. 51.
- A. E. Siegman, *Lasers* (University Science, California, 1986), Chap. 20.
- J. D. Jackson, *Classical Electrodynamics*, 2nd ed. (Wiley, New York, 1975), Chap. 3, p. 131.
- J. E. Sipe, "The dipole antenna problem in surface physics: a new approach," *Surf. Sci.* **105**, 489–504 (1981).
- M. Nahata, A. S. Weling, and T. F. Heinz, "A wideband coherent terahertz spectroscopy system using optical rectification and electro-optic sampling," *Appl. Phys. Lett.* **69**, 2321–2323 (1996).
- E. D. Palik, ed., *Handbook of Optical Constants of Solids* (Academic, Orlando, Fla., 1985).
- A. E. Siegman, *Lasers* (University Science, California, 1986), p. 637.
- P. Y. Han and X.-C. Zhang, "Coherent, broadband midinfrared terahertz beam sensors," *Appl. Phys. Lett.* **73**, 3049–3051 (1998).
- G. Gallot and D. Grischkowsky, "Electro-optic detection of terahertz radiation," *J. Opt. Soc. Am. B* **16**, 1204–1212 (1999).
- A. Leitenstorfer, S. Hunsche, J. Shah, M. C. Nuss, and W. H. Knox, "Detectors and sources for ultrabroadband electro-optic sampling: experiment and theory," *Appl. Phys. Lett.* **74**, 1516–1518 (1999).
- H. J. Bakker, G. C. Cho, H. Kurz, Q. Wu, and X.-C. Zhang, "Distortion of terahertz pulses in electro-optic sampling," *J. Opt. Soc. Am. B* **15**, 1795–1801 (1998).
- A computer implementation of the calculations in C/C++ can be obtained at <http://www.novajo.ca/thzcode.html>.